

Chapter 1

The atmospheric wave–turbulence jigsaw

Michael E. McIntyre

Dept. of Applied Mathematics & Theoretical Physics, University of Cambridge

To appear in *Rotation and Momentum Transport in Magnetised Plasmas*

edited by P. H. Diamond, X. Garbet, P. Ghendrih, Y. Sarazin. World Scientific (2012)

(Draft revised 14 February 2012)

1.1 Introduction

It was a great honour to be asked to give the Marshall Rosenbluth Memorial Lecture. Having never worked on plasma physics, though, I also feel some diffidence! The closest I've ever come has been involvement in some peculiar MHD problems that promise an improved understanding of the solar tachocline — more about confining a magnetic field within a plasma than a plasma within a magnetic field. Before proceeding I want to thank Drs Laurène Jouve and Chris McDevitt for producing the first draft of this chapter following my lecture. Chris also kindly lent assistance with the source files and graphics. However, the final responsibility for this chapter and any errors it may contain is mine alone.

What I do know something about is the kind of fluid dynamics that has helped us to understand the Earth's atmosphere and oceans. We still have an enormous phase space, but for classical fluid dynamics it has fewer degrees of freedom than for plasma physics. Thanks to countless observations and to the peculiarities of fluid flow heavily constrained by Coriolis effects and stable density stratification, considerable progress has been made in penetrating the nonlinear dynamics. Indeed, and quite surprisingly, researchers into atmosphere–ocean dynamics have gained insight in a way that cuts straight to strong nonlinearity, avoiding the standard paradigms. And an even greater surprise, to me at least, has been what Pat Diamond, Paul Terry and others have been saying in recent years — building especially

on the classic work of Hasegawa, Mima, and Wakatani — namely that some of the insights from atmosphere–ocean dynamics are relevant to some aspects of plasma behaviour in tokamaks, especially the self-organizing zonal flows that appear so important for plasma confinement; see, e.g., [1], [2], and references therein.

The standard paradigms avoided include those of weak nonlinearity, strong scale separation, “cascades” in the strict sense of being local in wavenumber space, and indeed homogeneous turbulence theory in all its flavours. Ever since the 1980s when infrared remote sensing from space began to give us global-scale views of, especially, stratospheric fluid flow, it has become apparent we are dealing with a highly inhomogeneous “wave–turbulence jigsaw puzzle” with no scale separation but with weakly and strongly nonlinear regions closely adjacent and intimately interdependent [3], [4]. One of the tools that have helped us to make sense of this has been the finite-amplitude “wave–mean interaction theory” developed over many years and recently summarized in a beautiful new book by my colleague Oliver Bühler [5].

For instance a typical phenomenon, once completely mysterious but now well understood, and understood in a very simple way, is the self-organization and the peculiar persistence and quasi-elasticity of the great atmosphere–ocean jet streams. They can persist over surprisingly large distances. If ordinary, domestic-scale jets behaved similarly, you could blow out your birthday candles from the far end of the room. There are “antifrictional” effects that prevent the great jets from spreading out dissipatively, and tend to re-sharpen their velocity profiles if something smears them out. As recorded in the famous books by Edward N. Lorenz, the father of chaos theory, and Victor P. Starr, the pioneer of postwar global upper-air data analysis, this behaviour used to be called “negative viscosity” and was regarded as a profound enigma [6], [7]. Such was the state of things when I became Jule Charney’s postdoc at MIT in the late 1960s.

The most conspicuous jets include of course the Gulf Stream, the Kuroshio Current, and the atmospheric jet streams that are typically found at airliner cruise altitudes, rivers of fast-flowing air a few kilometres deep and a few hundred kilometres wide, roughly speaking. As airline operators know very well, these atmospheric jet streams — which are among the most comprehensively observed of natural phenomena — can persist for thousands of kilometres and can have wind speeds sometimes exceeding even 100 m s^{-1} or 200 knot. The cores of these thin jets may meander, river-like, with large amplitudes, but nevertheless form resilient, flexible barriers

to the turbulent transport of material *across* them — by contrast with the high-speed advective transport *along* them — making the jets almost the “veins and arteries of the climate system”. Equally spectacular, though far less well understood, are the jets and associated transport barriers in the visible weather layer of the planet Jupiter.

I find myself wondering whether tokamak zonal flows are closer to the terrestrial or Jovian cases. Our relatively poor understanding of Jupiter makes this a hard question to answer at present. For Jupiter there are relatively few observational constraints, apart from the wind fields derived from cloud-top motions and the peculiar straightness of the jets that makes them, as it were, so conspicuously unearthly. It might be good news if the zonal jets in big tokamaks were more Jupiter-like than Earth-like, because less meandering might mean better confinement.

It cannot be too strongly emphasized that, for all the prolific literature, our understanding of the Jovian problem is indeed in its infancy. For one thing, progress has been impeded by a tendency to forget that in the real planet, as distinct from many models of it that have been studied, there is no solid surface or phase change sufficiently near the visible surface to support the type of baroclinic instabilities that excite terrestrial atmospheric jets. There is a “convective thermostat” mechanism — see [8] and references therein — that pretty much precludes any major role for such baroclinic instabilities. And our understanding of the most basic aspect of all, namely the coupling between Jupiter’s weather layer and the underlying convection zone, is very poor indeed. Here, however, there are signs of impending paradigm changes. But let me come back to Earth and to things about which we know more.

1.2 On eddy-transport barriers

The turbulent transport inhibition or “eddy-transport barrier” effect at jet cores goes hand-in-hand with the antifrictional effects. It depends on the strong, self-maintaining horizontal shears adjacent to the jet core as well as on the *potential-vorticity gradients* — see below — that are concentrated at the jet core. The importance of shear was pointed out in [9]. So although we used to speak of “potential-vorticity barriers”, the tendency in the atmosphere-ocean community these days is to call them “eddy-transport barriers”. Their dynamics involves both wave propagation and turbulence — strongly nonlinear and strongly inhomogeneous spatially,

with no spatial scale separation. As already hinted, this is far beyond the reach of both homogeneous turbulence theory and weakly-nonlinear wave or weak-turbulence theory.

The eddy-transport-barrier effect has been demonstrated again and again from observations, from laboratory experiments, and from high-resolution numerical models. An early and very striking observational demonstration came from studies of the radioactive debris from atmospheric nuclear tests published in 1968. Using an instrumented aircraft, two air masses well characterized by differing radioactive properties were observed flowing side by side in close proximity, without mixing, on either side of a jet core [10].

Another striking demonstration came from a laboratory experiment in Harry Swinney's big rotating tank at the University of Texas at Austin [11], [12]; see Fig. 1.1. Dye injected on one side of a jet stayed there, after more than 500 tank revolutions — almost perfectly confined despite the large-amplitude undulation of the jet. The jet core and velocity maximum were found to be almost coincident with the dye boundary.

And again, there has been a huge amount of observational and numerical modelling work in connection with the concern over ozone hole in the Antarctic stratosphere, where the polar-night jet, or polar-vortex edge, keeps itself sharp and acts as an eddy-transport barrier within which the ozone chemistry proceeds differently from the chemistry outside. This has been studied using intensive observations and a large hierarchy of models for over two decades now; among the many landmarks we may note a remarkable pair of papers by Norton [13] and Waugh and Plumb [14]. My website has a movie from Norton's work that visualizes the barrier effect rather spectacularly — websearch "**dynamics that is significant for chemistry**".

One might ask why there should be any comparison between the above-mentioned laboratory experiment and the atmosphere. Admittedly both are rapidly-rotating systems, in the sense that Coriolis effects are strong. However, stable stratification is very important in the atmosphere, and in the oceanic examples too, whereas the laboratory experiment used an unstratified fluid. The answer is, I've always thought, a rather surprising one. The kind of dynamics involved in all these systems has the same generic structure, explaining the many qualitative similarities between the systems. Even more surprisingly, the same generic structure is found in the tokamak models of Hasegawa, Mima and Wakatani. As we'll see, it is well illustrated by the simplest such model defined by the Hasegawa–Mima

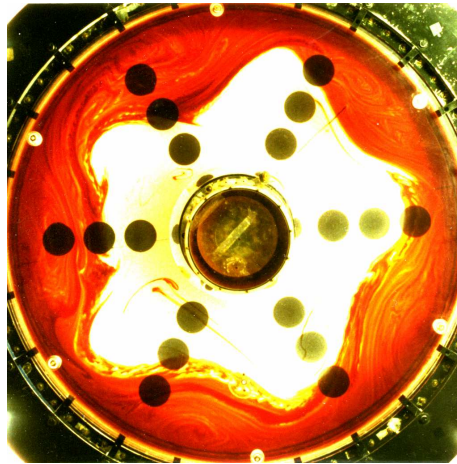


Fig. 1.1 From the laboratory study of Sommeria et al. [11]. Courtesy Dr Joël Sommeria.

equation (Sec. 1.8 below). And it is this structure that allows the insight into strong nonlinearity.

1.3 The generic dynamics

The generic dynamics is shared by a whole hierarchy of models of stratified, rotating atmosphere–ocean dynamics and their unstratified laboratory counterparts, including some remarkably accurate stratified models that easily explain, for instance, the characteristic cross-sectional structure of jet streams that has long been familiar to observational meteorologists [15], [16]; see Fig. 1.3 below. In all these models one has a single scalar field $Q(\mathbf{x}, t)$ that is a *material invariant* for ideal fluid flow, expressing the advective nonlinearity in a way that is easy to understand and to visualize. And more than that, the evolution of the Q field captures *everything* about the advective nonlinearity because, to the extent that these models are accurate, the Q field contains all the dynamical information at each instant. So if for example $\mathbf{u}(\mathbf{x}, t)$ is the velocity field, which for definiteness we'll take relative to the rotating Earth, then \mathbf{u} can be deduced at each instant from the Q field alone.

Q is called the *potential vorticity* of the model, and the mathematical process of deducing the \mathbf{u} field from the Q field is called *PV inversion*. The hierarchy of models arises because there is an array of different PV inver-

sion operators. They are inverse elliptic operators, hence nonlocal. They differ among themselves for two reasons. One is simply to accommodate the different physical systems that might be of interest, for example the atmosphere, or the laboratory system of Fig. 1.1, or the tokamak. The other is that, for a given physical system, some PV inversion operators are more accurate than others. In atmosphere–ocean dynamics, at least, there is always a tradeoff between simplicity and accuracy. Anyone who is curious as to what a highly accurate inversion operator looks like — the technicalities are nontrivial — may consult a little review that I wrote recently for *Advances in Geosciences* [17]. The property shared by the whole hierarchy, that the Q field contains all the dynamical information, is sometimes called the PV “invertibility principle”.

Using the notations $D/Dt := \partial/\partial t + \mathbf{u} \cdot \nabla$ for the material derivative and \mathcal{I} for the inversion operator, we can write the generic dynamics in great generality as the following pair of equations:

$$DQ/Dt = \text{forcing} + \text{dissipation} , \quad (1.1a)$$

$$\mathbf{u}(\mathbf{x}, t) = \mathcal{I}[Q_a(\cdot, t)] , \quad (1.1b)$$

where $Q_a(\mathbf{x}, t)$ is the PV anomaly field relative to a background state at relative rest in the rotating system, $\mathbf{u} \equiv 0$, whose PV is Q_b , say:

$$Q_a := Q - Q_b \quad (1.1c)$$

The dot in (1.1b) signals that the inversion operator acts nonlocally on the Q_a field. We have $\mathcal{I}[Q_a] \equiv 0$ if and only if $Q_a \equiv 0$ everywhere.

PV inversion is a diagnostic, as distinct from a prognostic, operation. Diagnostic means that (1.1b) contains neither time derivatives nor history integrals. The single time derivative in (1.1a) is the only time derivative in the problem. The forcing and dissipation terms in (1.1a) will of course depend on the particular physical system and model assumptions, but may often be considered small for practical purposes.

The single time derivative has strange and interesting consequences. It tells us at once that the only possible wave propagation in this kind of system will be one-way propagation, in the sense that the dispersion relation can have only a single frequency branch. These are the famous westward-propagating Rossby or vorticity waves of atmosphere–ocean dynamics and the equally famous electrostatic drift waves of tokamak dynamics, arising from gradients in the background state Q_b . The waves seen in Fig. 1.1 are Rossby waves. They are very different from the classical types of waves

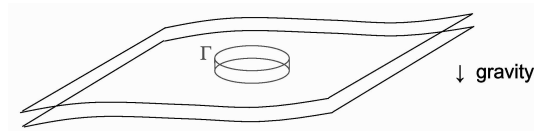


Fig. 1.2 Two stratification surfaces $\theta = \text{constant}$ in stratified, rotating flow. The material invariance of Q for ideal-fluid flow, essentially the constancy of absolute Kelvin circulation for a material circuit Γ lying in a stratification surface, exactly captures how the component of vorticity normal to each stratification surface changes under vortex stretching and vortex tilting.

we are all brought up on, which have pairs of opposite-signed dispersion-relation branches reflecting time reversibility. Rossby and drift waves have their own peculiar arrow of time.

How do these waves know which way to go? In the atmosphere–ocean case it’s in part because they notice which way the Earth, or the laboratory tank, is rotating. In the tokamak case, they notice which way the azimuthal magnetic field component is pointing, along with the facts that the ions are positively charged and much heavier than electrons and that there’s a background density gradient. This one-wayness has consequences reaching far beyond small-amplitude wave theory. The single time derivative in (1.1a) is still there, no matter how strongly nonlinear things become.

Of the various definitions of Q the most accurate and general, in atmosphere–ocean dynamics, can be stated as follows. Up to a constant normalizing factor, Q is the absolute Kelvin circulation around an infinitesimally small circuit Γ lying in a stratification surface. That is, Q is proportional to the loop integral $\oint_{\Gamma} (\mathbf{u} + \boldsymbol{\Omega} \times \mathbf{x}) \cdot d\mathbf{x}$ where $\boldsymbol{\Omega}$ is the Earth’s angular velocity. Stratification surfaces are surfaces of constant θ , where θ is a thermodynamical material invariant for ideal-fluid flow, more generally

$$D\theta/Dt = \text{forcing} + \text{dissipation}. \quad (1.2)$$

For instance we can take θ to be the specific entropy or the so-called potential temperature. Figure 1.2 shows two of the stratification surfaces, which are usually close to horizontal in practice. Also shown are two of the small circuits Γ . The material invariance of Q for ideal-fluid flow, i.e. (1.1a) with right-hand side exactly zero, is an immediate corollary of Kelvin’s circulation theorem. In the ideal-fluid limit, (1.2) also has right-hand side zero and the stratification surfaces become material surfaces; so the Γ ’s can be taken as material circuits and Kelvin’s circulation theorem applies.

An equivalent definition of Q can be written in terms of the mass density

field ρ , the absolute vorticity $2\boldsymbol{\Omega} + \nabla \times \mathbf{u}$ and the stratification field θ as follows:

$$Q := \rho^{-1}(2\boldsymbol{\Omega} + \nabla \times \mathbf{u}) \cdot \nabla \theta . \quad (1.3)$$

Let $\Delta\theta$ be the θ -increment between the two stratification surfaces, taken infinitesimally small, and Δm the mass of the infinitesimally small pillbox-shaped fluid element defined by the pair of Γ 's in Fig. 1.2. Using Stokes' theorem we see that (1.3) is the Kelvin circulation multiplied by $\Delta\theta/\Delta m$. For ideal-fluid flow $\Delta\theta$, Δm , the Kelvin circulation and hence (1.3) are all exact material invariants. Yet another demonstration starts with the vorticity equation, i.e. the curl of the momentum equation, taking its scalar product with $\nabla\theta$ to annihilate the baroclinic vector product $\nabla\rho \times \nabla p$ involving the pressure p . This is the route taken in most textbooks.

In the unstratified laboratory case, almost the same picture applies except that the two stratification surfaces in Fig. 1.2 are replaced by the top and bottom boundaries of the tank. The layer now has finite thickness, a function of radius in the case of Fig. 1.1. But because there is no stratification the rapid rotation of the tank keeps the flow approximately two-dimensional — the so-called Taylor-Proudman effect — causing the material circuits Γ to move in parallel and the absolute Kelvin circulation around them to be function of time and horizontal position only.

Historically, the central importance of Q to atmosphere–ocean dynamics was first recognized by Carl-Gustaf Rossby in his seminal papers of 1936 and 1940 [18], [19], following the earlier demonstration by Vilhelm Bjerknes that Kelvin's circulation theorem is valid on a stratification surface. Rossby presented hydrostatic variants of the formula (1.3). The exact formula (1.3) was first published by Hans Ertel in 1942 [20], after a visit to Rossby's group in 1938. The PV invertibility principle began to be articulated in the late 1940s, in seemingly different though actually equivalent ways, through the work of Jule Charney [21], Aleksandr Mikhailovich Obukhov [22], and Ernst Kleinschmidt [23].

1.4 Cyclone and jet structure

To complete the generic picture we need a qualitative feel for what PV inversion is like. Illustrative formulae are given in Sec. 1.8; but one way to gain generic insight is to say that on each stratification surface the operator \mathcal{I} delivers a horizontal velocity field \mathbf{u} qualitatively like the electric field

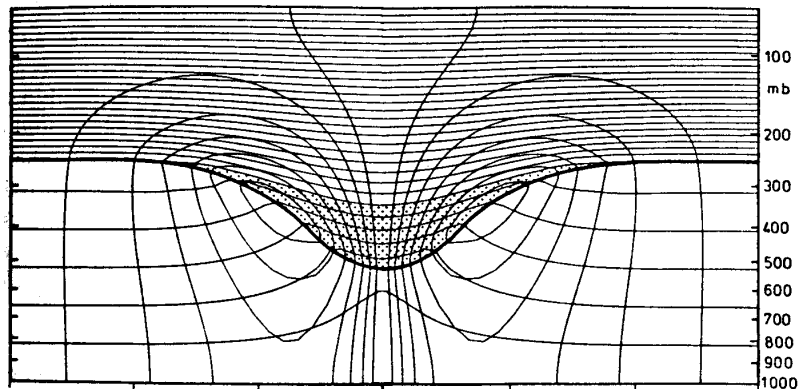


Fig. 1.3 Vertical section through an axisymmetric model of an upper-air cyclone; see text. Calculation by Dr A. J. Thorpe, from the review [24]. The entire structure comes from inverting a single positive PV anomaly located in the central stippled region. The heavy curve is the model tropopause, and the closed contours show the wind-speed profile, typical of atmospheric jets. Stronger jets go with steeper, or even reversed, tropopause slopes, but their structure is otherwise similar.

\mathbf{E} in a horizontally two-dimensional electrostatics problem, but rotated through a right angle, with Q_a in the role of minus the excess charge density. In the tokamak case with background magnetic field \mathbf{B} this is no accident, because in that case \mathbf{u} is proportional to $\mathbf{E} \times \mathbf{B}$ where \mathbf{E} really *is* the electric field! (Of course “horizontal” then corresponds to a cross-sectional plane of the tokamak, with \mathbf{B} nearly “vertical”.)

In realistic, stably-stratified atmospheric models, the electrostatic picture is only a rather rough, partial analogy, though still insightful. I believe it was first put forward by Obukhov. The notional electrostatics is “layerwise-two-dimensional” insofar as one takes the horizontal component of \mathbf{E} on each stratification surface and ignores the vertical component. The rotation of \mathbf{E} about the vertical to get \mathbf{u} is in a clockwise sense when viewed from above, i.e. compass-wise, in the northern hemisphere, corresponding to upward \mathbf{B} . However, thanks to Coriolis effects the field corresponding to the electrostatic potential needs to be calculated in three dimensions, inverting an elliptic operator resembling a modified three-dimensional rather than two-dimensional Laplacian, e.g. Eq. (1.6c) below. Thus the flow on one stratification surface is influenced by the notional charge distributions Q_a on other such surfaces over a significant depth of the atmosphere.

Figure 1.3 refines this rough picture by showing the result of an *accurate* three-dimensional inversion, taken from the 1985 review by Hoskins et al

[24]; q.v. for technical detail. The exact (Rossby–Ertel) Q field (1.3) has an axisymmetric positive anomaly¹ located in the central stippled region. In the electrostatic analogy we can think of it as a concentration of negative charge, making \mathbf{E} point inward. The heavy curve represents the tropopause, dipping down from altitudes around 10km down to 5km, corresponding to pressure-altitudes (right-hand scale) ranging from around 250 to 500 millibar. The stratification surfaces $\theta = \text{constant}$ are the light curves that tend toward the horizontal at the periphery. They are more crowded above the tropopause, i.e. in the stratosphere which, as its name suggests, is more stably stratified, increasing the magnitude of $|\nabla\theta|$ in (1.3). The vertical scale is stretched in the conventional way, to make the structure visible. In this case, which uses realistic atmospheric parameter values, the horizontal extent of Fig. 1.3 is 5000 km. So the stratification surfaces are actually very close to being horizontal.

The remaining light curves in Fig. 1.3 are the contours of constant wind speed, into the paper on the right and out of the paper on the left as expected from the inward-pointing \mathbf{E} vector in the layerwise-two-dimensional electrostatic analogy. The maximum wind speed occurs at the tropopause around 8km altitude, showing a jet structure that is very typical. In this case the maximum wind speed has a rather modest value, just over 20 ms^{-1} . Stronger PV anomalies produce stronger jets with the same structure except that the tropopause, defined as the PV anomaly boundary, tends to slope more steeply and indeed can become vertical or overturned, producing what is famously called a “tropopause fold”, e.g. Fig. 9b of [24].

I should explain that in order to do the inversion in this kind of problem one has to prescribe the mass under each stratification surface. That is how one tells the model to have a stratosphere with larger values of $|\nabla\theta|$ than the troposphere beneath [24]. One also has to impose what is called a *balance condition*. In this case it is enough to say that the flow is in hydrostatic and cyclostrophic balance. Cyclostrophic means that horizontal pressure gradients are in balance with the Coriolis force plus the centrifugal force $|\mathbf{u}|^2/r$ of the relative motion where r is horizontal distance from the symmetry axis. Thus pressures p are low at the centre of the structure.

¹As explained in the review [24], accurate inversion operators \mathcal{I} require the anomaly Q_a — there referred to as an “IPV anomaly” — to be defined relative to values on the same stratification surface $\theta = \text{constant}$, or “isentropic surface” in atmospheric-science language. This term arises because θ can be taken to be the specific entropy. So “IPV anomaly” means “isentropic anomaly of PV”. In the example of Figure 1.3 the positive anomaly is due mainly to the large magnitude of the factor $\nabla\theta$ in (1.3), i.e. to the presence of stratospheric rather than tropospheric air, in the central stippled region.

Although it is left implicit in (1.1b), inversion delivers the p , ρ and θ fields as well as the \mathbf{u} field, as the invertibility principle says it must. In more complicated, non-axisymmetric cases, accurate balance conditions can still be imposed over a surprisingly large range of parameter values, but at the cost of becoming technically much more complicated; see [17] and references therein.

Notice the power of the invertibility principle. The entire structure in Fig. 1.3, long familiar and easily recognizable from the zoological annals of observational meteorology — under such names as “upper-air cutoff cyclone” or “cutoff low”, e.g. Fig. 8 of [24] — follows from having just a single positive PV anomaly on stratification surfaces intersecting the tropopause. “Cutoff” refers to the way in which such PV anomalies are formed in reality, by a mass of high- Q stratospheric air being advected into lower- Q surroundings and then wrapping itself up into a cyclonic vortex (e.g. the coloured air over the Balkans in Fig. 1.4 below, also examples in [24]). The idea that a PV anomaly can wrap *itself* up makes perfect sense if the invertibility principle holds.

As already suggested, the jet structure illustrated in Fig. 1.3 is typical and very robust, over a large range of jet speeds and tropopause steepnesses. Although the example in Fig. 1.3 is idealized as being axisymmetric, one gets the same jet structure in more complicated cases whenever there is a concentrated gradient of Q on stratification surfaces, with high values adjacent to low values. The way in which such gradients arise — and observations repeatedly show that they are commonplace — is precisely through the strong nonlinearity I have been hinting at. Indeed, the way in which the concentrated gradients arise can be viewed as a rather simple kind of strongly-nonlinear *saturation*. The oft-observed jet structure is telling us that, in reality, saturated states are often approached.

It is worth pointing out for later reference that even without relative motion \mathbf{u} there may well be pre-existing *large-scale* gradients in Q_b , the background PV distribution. For the tokamak they come from the radial temperature and density gradients. For realistic atmosphere-ocean dynamics they come from the fact that, in the formula (1.3), horizontal stratification surfaces pick out the vertical component, f say, of the planetary vorticity $2\boldsymbol{\Omega}$. At latitude λ we have to good accuracy

$$f = 2|\boldsymbol{\Omega}| \sin \lambda; \quad (1.4)$$

f is called the Coriolis parameter. Its northward gradient is conventionally denoted by β and also by the phrase “beta effect”, not to be confused with

plasma beta.

Before leaving this topic I should point out that if one wants to cover a wider range of significant cases then one has to count as part of the Q field the distribution of θ at the Earth's surface. This last behaves somewhat like a Dirac delta function in the vertical distribution of Q , and is important in some dynamical processes. A prime example is the baroclinic instability and the associated wrapping-up and "frontogenesis" in the surface- θ field that's so important in the terrestrial atmosphere [25], though not in the Jovian. The Earth's large-scale surface- θ gradient across latitudes provides an effective *southward* PV gradient, opposing that of the beta effect and mediating a powerful shear instability. The resulting frontogenesis in the surface θ distribution is another variation on the theme of saturation. Baroclinic instability is the atmosphere-ocean counterpart of plasma drift wave self-excitation by resistive instability.

1.5 Strong nonlinearity is ubiquitous

Why should concentrated PV gradients be so commonplace along with their inversion signatures, the great jet streams, and indeed surface fronts as well, and what justifies associating them with a saturation process? What produces the accompanying antifrictional or "negative viscosity" effects that used to be thought so mysterious? The answer lies in the idea of "PV mixing" — more precisely, in the idea of layerwise-two-dimensional regional turbulent PV mixing, the mixing of PV along stratification surfaces in certain regions. Such mixing is a strongly nonlinear process because it involves not just weak distortions or resonant-triad interactions but, rather, drastic advective rearrangements of large-scale into smaller-scale PV fields. Such regional or inhomogeneous PV mixing has the potential to weaken PV gradients in some places on stratification surfaces, and strengthen them in others to form jets and eddy-transport barriers; see Secs. 1.6–1.7 below.

Neither mixing nor eddy-transport barriers need be perfect. Indeed in many cases the vortex dynamics produces new coherent structures on different spatial scales, as illustrated in Fig. 1.4. On the other hand, whenever perfect or near-perfect mixing is achieved within some region, we have a rather *simple* kind of strongly nonlinear saturation because once we have a well-mixed region, further mixing has little further effect.

Equation (1.1a) with its advective nonlinearity tells us that we can, indeed, reasonably regard Q as a mixable quantity, to that extent like a chemical tracer. For early applications to real atmospheric phenomena see

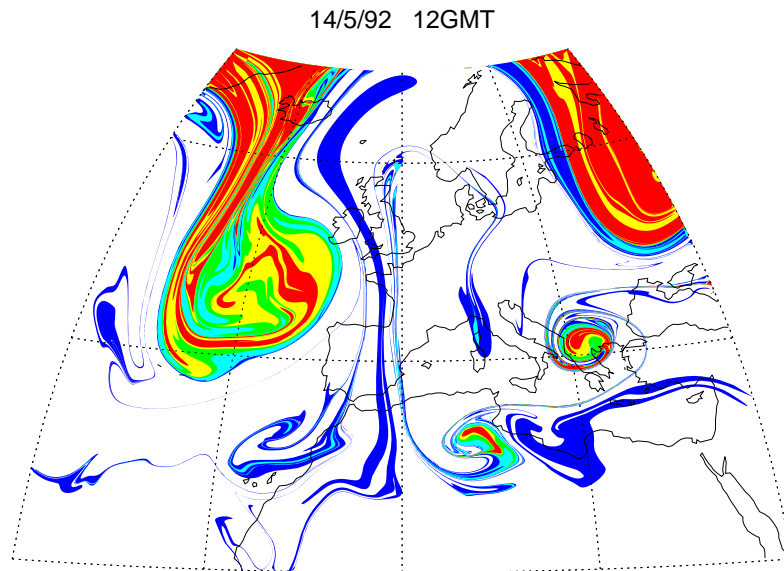


Fig. 1.4 Estimated map of Q on a stratification surface near 10km altitude, from [26]. The computation assumes that material invariance of Q is a good approximation over a 4-day time interval, and uses a state-of-the-art advection algorithm to trace the flow of high- Q stratospheric air (coloured) and low- Q tropospheric air (clear). The main boundary between stratospheric and tropospheric air marks a jet core showing large-amplitude meandering, from Greenland toward Spain and then back to northern Norway. The leakage of stratospheric air into the troposphere signals intermittent attrition of the eddy-transport barrier at the jet core. The different chemical signatures of the stratospheric and tropospheric air are easily detectable and have been demonstrated in measurement campaigns, even for fine filamentary structures like those shown [14]. The high- Q anomaly over the Balkans illustrates the “cutoff” or self-wrapping-up process that occurs when sufficiently large masses of stratospheric air overcome the barrier. The wrapping-up produces structures like that in Fig. 1.3.

[27]. Today the reality of PV mixing, and the tendency toward piecewise-saturated, piecewise-well-mixed states in many cases, has extremely strong observational support. That is one reason why we think of Eq. (1.1a) with small right-hand side as a key to understanding real atmospheric jets, upper-air cyclones, surface fronts and many other meteorological phenomena. For instance a spectacular example of a large, well-mixed area in the real winter stratosphere has been closely studied in [28]. A movie from that study is available on my website: websearch "gyroscopic pump in action". There are countless further examples at lower altitudes near the

tropopause, for instance those documented in [29].

A recent numerical model study [30] finesses these PV-mixing ideas through numerical experiments showing the co-development of jets, well-mixed areas and coherent vortices, with the vortices actively contributing to the mixing, an idealized version of Fig. 1.4. The discussion of strongly-nonlinear coherent structures in Diamond et al. (this volume) hints that we might end up with a similar picture for real drift-wave turbulence in large tokamaks.

Today we can routinely map the real atmospheric Q fields through the highly sophisticated (spacetime Bayesian) observational data-assimilation technology that underpins operational weather forecasting; see [4] for a state-of-the-art movie from that technology. Yet again, we see large regions on stratification surfaces within which Q is roughly constant as a result of mixing, bordered by concentrated gradients marking the eddy-transport barriers at jet cores. We can see the mixing taking place in more and more detail, over an increasingly large range of spatial scales as computer power increases. These situations are at an opposite extreme from those assumed in classical homogeneous turbulence theory. In a nutshell, reality is highly inhomogeneous.

The laboratory experiment of Fig. 1.1 tells the same story. Through careful measurements the experimenters were able to map the PV field appropriate to that system. The resulting PV maps [11], [12] closely resemble the dye pattern in Fig. 1.1, with well-mixed regions on either side of the jet core. Even though the visible wavy pattern might suggest the validity of linearized or weakly-nonlinear Rossby-wave theory, the suggestion is misleading because the fluid motion has already rearranged its PV distribution to be close to piecewise uniform on either side of the jet core, with a concentrated PV gradient at the core. Strong nonlinearity did most of its work before the dye was injected. At the instant shown in Fig. 1.1, mixing continues on either side of the jet but has become invisible, since there were no further dye injections. As far as the dynamics is concerned, the mixing process has saturated.

Figure 1.1 well illustrates what I mean by the “wave–turbulence jigsaw”. We have a wavy, weakly nonlinear jet-core region adjacent to strongly nonlinear regions on either side of the jet core.

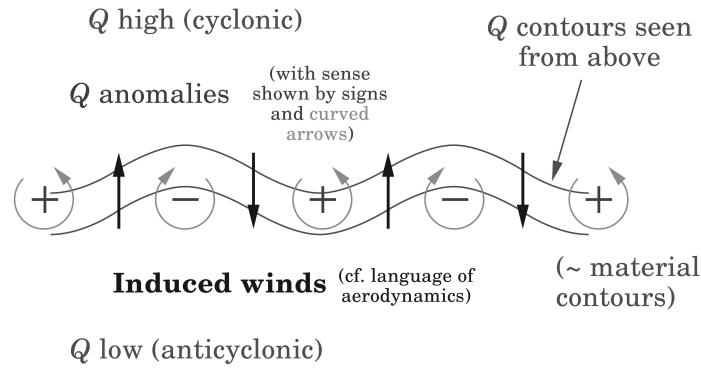


Fig. 1.5 Plan view of an x -periodic Rossby wave, where x points toward the right in the figure. The plus and minus signs respectively indicate the centres of the cyclonic and anticyclonic PV anomalies due to southward and northward air-parcel displacements across a basic northward PV gradient. For a tokamak drift wave, “cyclonic” means a vorticity vector pointing in the $+\mathbf{B}$ direction, toward the viewer in this case. The plus signs then correspond to *negative* net charge, and minimal density, and in the background gradients high Q corresponds to low background density.

1.6 Rossby waves and drift waves

Figure 1.5 shows the generic propagation mechanism for Rossby and drift waves. The background rotation $\boldsymbol{\Omega}$ and azimuthal magnetic field \mathbf{B} point toward the viewer. Propagation occurs whenever the Q field has a background gradient. We consider a background Q field $Q_b = Q_b(y)$, where in atmosphere-ocean cases we take y as pointing northward, in the direction of increasing Q_b , and in tokamak cases as pointing radially toward decreasing background mass density. The y direction is toward the top of the figure and the x direction toward the right; please note that this is not the usual coordinate convention for tokamaks. For the stratified atmosphere $dQ_b/dy > 0$ is the “isentropic” gradient, along a stratification surface.

With no disturbance the constant- Q contours would be straight and parallel to the x axis. We imagine that a small disturbance makes them wavy, as shown. We assume ideal-fluid motion, i.e., zero on the right of Eq. (1.1a). Then the wavy Q contours are also material contours. Linearized wave theory requires the undulations to be gentle: their sideways slopes must be much smaller than unity. We have a row of PV anomalies $Q_a = Q - Q_b$ of alternating sign, as suggested by the plus and minus signs enclosed by circular arrows. In the electrostatic analogy — be careful —

plus means a *negative* charge and vice versa. (If only the world were made of antimatter, it would be easier to be lucid here.)

Inversion gives a velocity field \mathbf{u} ($\propto \mathbf{E} \times \mathbf{B}$ for the tokamak) whose north-south component is a quarter wavelength out of phase with the north-south displacement field, as suggested by the big dark arrows in Fig. 1.5. (In the meteorological literature the velocity field resulting from a PV inversion is sometimes called the wind field “induced” by the PV anomalies.²)

So to understand Rossby-wave and drift-wave propagation — generically, and not just in textbook cases — one need only use one’s visual imagination to turn Fig. 1.5 into a movie. With velocity a quarter wavelength out of phase with displacement, the pattern will start to propagate to the left. But invertibility, Eq. (1.1b), says that the velocity pattern must remain phase-locked to the displacement pattern! So the propagation continues indefinitely. With the signs shown, the propagation is in the negative x direction — the famous westward, or quasi-westward, or high- Q -on-the-right phase propagation, relative of course to any mean flow. We may think of the Q contours as possessing a peculiar Rossby-wave “quasi-elasticity”. This shows up spectacularly in Norton’s movie mentioned in Sec. 1.2.

If we do a thought-experiment in which all the signs are changed in Fig. 1.5, replacing westward phase propagation by eastward, then we are describing the effect of the large-scale gradient in surface θ noted at the end of Sec. 1.4. The simplest and most powerful baroclinic-instability mode can be thought of as a pair of counterpropagating Rossby waves on the opposing interior and surface PV gradients, phase-locked with the help of the mean vertical shear [24].

The propagation mechanism works similarly for uneven Q contour spacing, including the case of a jet with most of the Q contours bunched up at the jet core. This means that jets can act as Rossby waveguides, with quasi-elastic cores. Figure 1.1 is an example. Some atmospheric examples are discussed in [29]. Explicit toy-model solutions will illustrate the same point in Sec. 1.11.

If the Q contours in Fig. 1.5 were deforming irreversibly rather than gently undulating, then we would say that the Rossby waves are *breaking*. Indeed, for strong reasons grounded in wave-mean interaction theory

²Here meteorologists are following the language of aerodynamics dating from the pioneering days of Frederick Lanchester and Ludwig Prandtl, where three-dimensional *vorticity inversion* using a Biot-Savart integral has long been a basic conceptual tool. As an aerodynamicist would put it, aeroplanes stay up thanks to the downward velocity “induced” by the trailing wingtip vortices.

we may regard such irreversible deformation as the defining property of wave breaking [5], [31]. In the atmosphere, at least, there is no doubt that the breaking of Rossby waves is Nature's principal way of causing PV mixing and its typical consequences, antifrictional jet sharpening and eddy-transport-barrier reinforcement. The associated radiation stress or wave-induced momentum transport is an essential part of how the jigsaw fits together [17], [32], [33]. One way of seeing more precisely how it fits together is through what is called the *Taylor identity*, or *Taylor-Bretherton identity*; see (1.9) and (1.10)ff. below.

In Sec. 1.11 we'll see that jet-guided Rossby waves have a strong tendency to break on one or both sides of the jet, leaving the jet core intact. That is, there is a systematic tendency for PV mixing to occur preferentially on the flanks of a jet — sharpening the jet antifrictionally, reinforcing the eddy-transport-barrier effect, and keeping the wave-turbulence jigsaw highly inhomogeneous. We may think of jets almost as *self-sustaining* elastic structures; the only help they need is for their Rossby waves to be excited now and again, for instance by baroclinic instabilities.

1.7 The PV Phillips effect

There is an even simpler, and independent, argument suggesting that the spatial inhomogeneity or regionality I keep talking about is generically likely. Imagine a large-scale, initially uniform PV gradient subject to random disturbances. Suppose that these disturbances produce PV mixing, slightly stronger in some regions than others. The regions where mixing is stronger will have their overall PV gradients weakened. But then those regions will have weaker Rossby-wave quasi-elasticity, and will be even easier to mix. Other things being equal, there is a positive feedback that tends to push the contours apart in some regions and bunch them together in others.

I like to call this the "PV Phillips effect", after O. M. Phillips' original suggestion in 1972 that the same thing happens with vertical gradients of θ , i.e. with stable stratification [34]; see also [32], [35] and references therein. In that case the suggestion was beautifully verified in a non-rotating, stratified laboratory tank experiment [36]. One starts with the uniform stratification created by a smooth vertical gradient of salinity. Salinity is a convenient laboratory counterpart to θ , or rather to $-\theta$ because more salinity means more density and less buoyancy. One stirs the tank with smooth vertical rods. This imposes no vertical scale of motion smaller

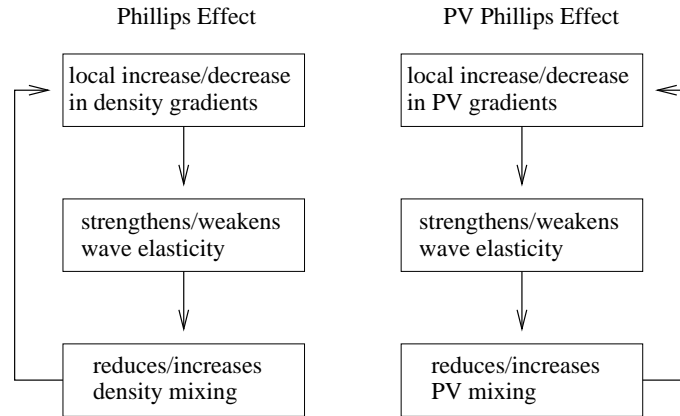


Fig. 1.6 Schematic of the positive feedback loops for the original Phillips effect and its PV counterpart. Courtesy of Drs Jouve and McDevitt. In the PV case the positive feedback is reinforced by jet shear, leading to the formation of eddy-transport barriers such as that illustrated in Fig. 1.1. Further reinforcement can come from the preferred phase speeds of disturbances, as discussed in Sec. 1.11.

than the depth of the tank. Nevertheless the stratification rearranges itself into horizontal layers. Layers with weak stratification, relatively small $|\nabla\theta|$, are sandwiched between horizontal interfaces with strong stratification, relatively large $|\nabla\theta|$. The vertical scale depends on how vigorously one stirs. With sufficiently vigorous stirring one can of course homogenize the whole tank. Otherwise, we have — guess what — yet another example of the tendency for real turbulence to be highly inhomogeneous and for eddy-transport barriers to form.

The original Phillips effect and its PV counterpart are summarized in Fig. 1.6, courtesy of Drs Jouve and McDevitt. In the original Phillips effect the relevant wave elasticity is that associated with internal gravity waves, the waves that owe their existence to the stable stratification $\nabla\theta$.

In the case of PV the positive feedback tends to be reinforced by the shear effects [9], [32], contributing to eddy-transport-barrier formation as suggested in Sec. 1.2. It turns out that the shearing of small-scale disturbances is just as important as the Rossby-wave quasi-elasticity felt by larger-scale disturbances. There is a *scale effect*, coming from the inversion operator, that weakens the \mathbf{u} field of the smallest-scale PV anomalies. So the small-scale behaviour tends to be passive-tracer-like, as indeed was suggested by the filamentary structures in Fig. 1.4.

1.8 Some simple inversion operators

To check our insights we often use models with simplified but qualitatively reasonable inversion operators \mathcal{I} . The most important of these models are the so-called *quasi-geostrophic* models. They are not quantitatively accurate but are conceptually important because their dynamics still has the generic form (1.1a)–(1.1c) and, at a good qualitative level, they describe phenomena such as the scale effect, Rossby-wave propagation, and Rossby-wave breaking and other strongly nonlinear phenomena such as vortex interactions and so-called “cascades”. Inversion, which generically speaking is a mildly nonlinear operation, albeit a smoothing operation because of the scale effect, becomes strictly linear in these models. This allows free use of the superposition principle and helps to expand the repertoire of explicit illustrative solutions. The advective nonlinearity is the only nonlinearity. The quasi-geostrophic models come in a number of versions, including single-layer, multi-layer, and continuously stratified. The standard single-layer or “shallow-water” version is isomorphic to one version of the Hasagawa–Mima tokamak model.

The term quasi-geostrophic comes from the balance condition used to construct the inversion operator \mathcal{I} , simple geostrophic balance, in which we entirely neglect the relative centrifugal and other small nonlinear terms in the hierarchy of more accurate balance conditions. Geostrophic balance means balance between Coriolis forces and horizontal pressure gradients. This is a valid asymptotic approximation in the limit of small Rossby number $\text{Ro} := f^{-1} |\hat{\mathbf{z}} \cdot \nabla \times \mathbf{u}|$ where f is the Coriolis parameter as before, and $\hat{\mathbf{z}}$ a unit vertical vector.

In these models it is convenient to use modified definitions of the PV, to be denoted by q , with background q_b . Within the asymptotic approximation schemes that lead to the models, which originated in the independent pioneering work of Charney [21] and Obukhov [22] and are described in many textbooks, we may regard the velocity field as purely horizontal and nondivergent to leading order. An $O(\text{Ro})$ correction is implicit, allowing weak vertical motion and horizontal divergence. So to leading order we can introduce a streamfunction $\phi(\mathbf{x}, t)$, which is a suitably Coriolis-scaled pressure anomaly such that, to leading order, $\mathbf{u} = \mathbf{u}_g := \hat{\mathbf{z}} \times \nabla \phi = (-\phi_y, \phi_x, 0)$, expressing geostrophic balance. Suffixes x and y denote partial differentiation. In terms of the corresponding “geostrophic” material derivative $D_g/Dt := \partial/\partial t + \mathbf{u}_g \cdot \nabla$ the dynamics takes the form

$$D_g q/Dt = \text{forcing} + \text{dissipation} , \quad (1.5a)$$

$$\mathbf{u}_g(\mathbf{x}, t) = \mathcal{I}[q_a(\cdot, t)] := \hat{\mathbf{z}} \times \nabla \mathcal{L}^{-1} q_a , \quad (1.5b)$$

$$q_a := q - q_b , \quad (1.5c)$$

where \mathcal{L} is a linear elliptic operator given by the horizontal Laplacian $\nabla_H^2 = \partial_{xx} + \partial_{yy}$ plus extra terms that vary from model to model. These operators have well-behaved inverses \mathcal{L}^{-1} given reasonable boundary conditions. Of course (1.5b)–(1.5c) amount to saying that in each case the definition of q is $q_b + \mathcal{L}\phi$. However, saying it via (1.5b)–(1.5c) clarifies that these models are indeed examples of the generic dynamics.

Examples include the following three. The first two are single-layer, two-dimensional models with $\phi = \phi(x, y, t)$, involving a fixed lengthscale L_D to be specified shortly. The third is three-dimensional with $\phi = \phi(x, y, z, t)$, taking account of continuous background stratification:

$$\text{Model 1: } \quad \mathcal{L}\phi := \nabla_H^2 \phi - L_D^{-2} \phi , \quad (1.6a)$$

$$\text{Model 2: } \quad \mathcal{L}\phi := \nabla_H^2 \phi - L_D^{-2} \tilde{\phi} , \quad (1.6b)$$

$$\text{Model 3: } \quad \mathcal{L}\phi := \nabla_H^2 \phi + \frac{1}{\rho_0} \frac{\partial}{\partial z} \left(\frac{\rho_0 f_0^2}{N^2} \frac{\partial \phi}{\partial z} \right) . \quad (1.6c)$$

The tilde in model 2 denotes the departure from a zonal or x -average, $\tilde{\phi} := \phi - \langle \phi \rangle$. The continuous background stratification in model 3 is represented approximately in terms of background profiles $\rho = \rho_0(z)$ and $\theta = \theta_0(z)$, with the buoyancy frequency $N(z)$ defined in terms of the gravity acceleration g by $N^2 := g d \ln \theta_0 / dz$. Coriolis effects are represented by a domain-average Coriolis parameter $f = f_0 = \text{constant}$. In model 1 the lengthscale L_D , called the Rossby deformation length, is f_0^{-1} times the gravity-wave speed for the layer, which has a free top surface. More precisely, one uses the notional gravity-wave speed that would apply if f_0 were zero, measuring the quasi-static free-surface gravitational elasticity. The L_D term in model 1 expresses hydrostatic balance together with vortex stretching by the implicit vertical motion, essentially the ballerina effect from the accompanying horizontal convergence.

Model 2 is exclusive to the tokamak, having no atmosphere–ocean counterpart beyond its conformity to the generic dynamics. The ballerina effect is replaced by spinup via the magnetic Lorentz force $\mathbf{u} \times \mathbf{B}$ when ions

converge, \mathbf{u} being the ion flow component normal to the background magnetic field \mathbf{B} . Geostrophic balance is replaced by the leading-order balance $\mathbf{u} \times \mathbf{B} \approx -\mathbf{E}$, implying that the disturbance streamfunction $\tilde{\phi}$ is now $|\mathbf{B}|^{-1}$ times the disturbance to the electrostatic potential. In other words the Coriolis parameter is replaced by $|\mathbf{B}|$ and the pressure-gradient force by the electrostatic force. The ion pressure gradient ∇p_i and associated diamagnetic drift velocity $\propto |\mathbf{B}|^{-1} \hat{\mathbf{z}} \times \nabla p_i$ are relatively unimportant in the ion flow dynamics, ion temperatures being much lower than electron temperatures while electron and ion number densities are constrained to be approximately equal. Also implicit in the dynamics of model 2 are assumptions that the electrons are in thermal equilibrium (Boltzmann-distributed) at fixed high temperature T_e and that the disturbances $\tilde{\phi}$, while treated as two-dimensional in the cross-sectional plane of the tokamak, actually have a small but finite wavenumber component k_{\parallel} parallel to \mathbf{B} , allowing the electrons to adjust hydrostatically along the \mathbf{B} lines encircling the tokamak and making the flow in a single cross-sectional plane look more compressible than it would if $k_{\parallel} = 0$. The hydrostatically-balanced density fluctuation is proportional to $\tilde{\phi}$. This is the counterpart of the free-surface gravitational elasticity producing the finite L_D value in model 1. Also implicit in model 2 is an assumption that the zonal-mean flow $\langle \phi \rangle$ does, by contrast, have $k_{\parallel} = 0$, suppressing the electron-mediated compressibility and giving rise to the tilde in Eq. (1.6b).

Taking account of the charge-to-mass ratios for ions and electrons, one finds that the proportionality constants are such that the electron-mediated compressibility implies a lengthscale L_D in model 2 whose square is equal to the electron-to-ion mass ratio times v_e^2/ω_{ci}^2 , where v_e is the electrons' thermal speed and ω_{ci} is the ion gyrofrequency, which is $|\mathbf{B}|$ times the ions' charge-to-mass ratio. This L_D value is conventionally denoted by ρ_s and in practice is small in comparison with tokamak dimensions. It would become the ions' gyroradius if the ions were heated up to the much higher temperature of the electrons. The Rossby number is replaced by the small parameter $\omega_{ci}^{-1} |\hat{\mathbf{z}} \cdot \nabla \times \mathbf{u}|$. For the background PV gradient, the atmosphere-ocean β is replaced by ω_{ci}/L where L is the lengthscale of the background density gradient, with signs as in Fig. 1.5. Also, "forcing" in Eq. (1.5a) becomes the resistive self-excitation of drift waves [37], predominantly at scales of the order of $L_D = \rho_s$.

Model 3 requires a boundary condition $\phi_z = 0$ at a flat lower boundary, say $z = 0$, idealizing the Earth's surface. (In otherwise-unbounded domains we take evanescent boundary conditions.) For model 3 one can show from

hydrostatic balance that $\phi_z = g/f_0$ times the anomaly in $\ln \theta$ (ϕ_z having dimensions of velocity, like ϕ_x and ϕ_y). So the nonvanishing θ anomalies at $z = 0$ that are critical to baroclinic instability and frontogenesis correspond to nonvanishing ϕ_z at $z = 0$. However, as hinted at the end of Sec. 1.4 we can regard this situation as equivalent to $\phi_z = 0$ at $z = 0$ together with a compensating delta function in the last term of (1.6c), coming from a jump discontinuity in ϕ_z [38].

Since model 1 is often called the Hasegawa–Mima model or sometimes, for the sake of historical justice, the Charney–Obukhov–Hasegawa–Mima model, I’ll call model 2 with the tilde the “extended Hasegawa–Mima model”. Model 1 in its atmosphere–ocean applications is given the self-explanatory name “shallow-water quasi-geostrophic model” and sometimes, less transparently, “equivalent barotropic model”. Notice that we can turn model 3 into model 1 by imposing a fixed vertical structure with a single vertical scale H . Then a scale analysis applied to the term with the vertical derivatives gives $L_D = NH/f_0$, related to the notional internal-gravity-wave speed NH for $f_0 = 0$. Typical extratropical L_D values range between $\sim 10^3$ km– 10^2 km for the atmosphere and $\sim 10^2$ km– 10^1 km for the oceans.

Omitted from the list above are various two-layer and higher multi-layer models that also conform to the generic dynamics. They are essentially stacks of shallow water quasi-geostrophic models and are popular because they capture some aspects of continuous stratification, model 3, but with a reduced computational burden. There is a two-layer model that might, however, be worth exploration as an alternative to model 2 for the tokamak. In its atmosphere–ocean interpretation it represents a physically consistent thought-experiment with two L_D values, one finite and the other infinite, that might be put into correspondence with the tokamak’s finite- k_{\parallel} and zero- k_{\parallel} modes. It has been intensively studied.

The two-layer model’s finite or “baroclinic” L_D value arises from the gravitational elasticity of the interface between the layers, while the infinite or “barotropic” L_D value arises from rigid top and bottom bounding surfaces. This model has a large literature. Its main use has been to study the atmosphere’s baroclinic instability and the nonlinear consequences in the simplest possible setting, with the lower layer’s PV gradient as a surrogate for the real atmosphere’s surface- θ gradient, more accurately described by model 3. The resulting self-excited disturbances are drift-wave-like insofar as the excitation scale is, inevitably, the baroclinic L_D . They induce PV mixing and antifrictional momentum fluxes that excite zonal jets with

a significant or even dominant *barotropic*, $L_D = \infty$ component, corresponding to zero k_{\parallel} . (Contrary to common belief, no upscale energy “cascade” need be involved.) The barotropic and baroclinic components are defined as half the sum and half the difference of the velocity fields of the two layers. There is no space for further discussion here, but I would recommend reference [39] as lucid and insightful.

Taking $q_b = \beta y + \text{constant}$ as the background PV, with constant gradient β , we can easily check that models 1–3 possess waves that propagate in the manner sketched in Fig. 1.5. For instance both model 1 and model 2 linearized about relative rest have the same elementary wave solutions $\tilde{\phi} \propto \exp(ikx + ily - i\omega t)$ with the same, single-branched dispersion relation

$$\omega = \frac{-\beta k}{k^2 + l^2 + L_D^{-2}}, \quad (1.7)$$

where the denominator comes from $q_a = \tilde{q} = \mathcal{L}\tilde{\phi} = -(k^2 + l^2 + L_D^{-2})\tilde{\phi}$ in the linearized (1.5a) with right-hand side zero, $\partial\tilde{q}/\partial t + D_g q_b/Dt = \partial(\mathcal{L}\tilde{\phi})/\partial t + \beta\partial\tilde{\phi}/\partial x = 0$. Notice the scale effect: wave propagation is weakened as scales become smaller and $k^2 + l^2$ larger. In the long-wave limit $(k^2 + l^2) \rightarrow 0$ the phase velocity asymptotes to $-\beta L_D^2$, which in the tokamak case coincides with the background diamagnetic drift velocity, not of ions but of electrons. For barotropic or zero- k_{\parallel} modes, the denominator can become very small and this is sometimes referred to in the plasma literature as minimal “inertia”.

The laboratory flow in Fig. 1.1 has a rigid lid and is well described by model 1 with $L_D = \infty$. This is ordinary (Euler, inertial) two-dimensional vortex dynamics except that there is a nontrivial background $q_b = \beta y + \text{constant}$. This comes from a gently sloping cone-shaped tank bottom, where now y is radial distance toward the tank centre.

For model 1 in an unbounded domain with finite L_D one has the explicit inversion formula

$$\phi(\mathbf{x}, t) = \mathcal{L}^{-1}q_a := -\frac{1}{2\pi} \iint K_0\left(\frac{|\mathbf{x} - \mathbf{x}'|}{L_D}\right) q_a(\mathbf{x}', t) dx' dy' \quad (1.8)$$

where $|\mathbf{x} - \mathbf{x}'|^2 = (x - x')^2 + (y - y')^2$ and where K_0 is the modified Bessel function [22]. Its exponential decay shows that both linear and nonlinear interactions become very weak at distances significantly greater than L_D . Aphoristically speaking, we have action at a distance but not too great a distance, which helps to explain the surprising robustness of the generic dynamics [17] which, in effect, through the balance condition, assumes that

gravity-wave propagation is instantaneous. In model 2 this corresponds to instantaneous acoustic propagation in the thermalized electron gas.

1.9 Pseudomomentum and the Taylor identity

Models 1–3 and their multi-layer counterparts all possess what are called pseudomomentum theorems and Taylor or Taylor–Bretherton identities. All these theorems and identities stem from the seminal 1915 work of Sir Geoffrey Ingram Taylor [40] and its 1966 extension by Francis P. Bretherton [41]. (I count myself a direct intellectual descendent because Taylor was Bretherton’s PhD advisor and Bretherton was mine.) Taylor’s results apply to models 1 and 2; Bretherton carried out the extension to model 3, leading in turn to a milestone 1969 paper by Robert E. Dickinson [42]. Dickinson’s paper took what I regard as the decisive step toward solving the “negative viscosity” enigma for the real atmosphere, though further work was needed to see how simply it could be solved using the concept of Rossby-wave breaking. For more history see [32].

In their usual forms the pseudomomentum theorems depend on linearization and so apply to small-amplitude waves only. The Taylor and Taylor–Bretherton identities, by contrast, are valid at any amplitude, and so apply to the whole wave–turbulence jigsaw.

Consider an arbitrary zonal-mean state $\langle q \rangle = q_b + \langle q_a \rangle$. The non-background part $\langle q_a \rangle$ might for instance represent a jet flow. Take the disturbance part $\tilde{q} = \mathcal{L}\tilde{\phi}$ of (1.6a) or (1.6b). Multiply it by $\tilde{\phi}_x$ and take the zonal mean. The L_D terms disappear, because $\langle \tilde{\phi}_x \tilde{\phi} \rangle = \langle \frac{1}{2}(\tilde{\phi}^2)_x \rangle = 0$. From the horizontal Laplacian we have $\langle \tilde{\phi}_x \tilde{\phi}_{xx} \rangle = \langle \frac{1}{2}(\tilde{\phi}_x^2)_x \rangle = 0$ and so, noting also that $\langle \tilde{\phi}_{xy} \tilde{\phi}_y \rangle = \langle \frac{1}{2}(\tilde{\phi}_y^2)_x \rangle = 0$ and writing $\tilde{v} = \tilde{\phi}_x$, $\tilde{u} = -\tilde{\phi}_y$, dropping the suffix g from now on, we have

$$\langle \tilde{v} \tilde{q} \rangle = -\partial \langle \tilde{u} \tilde{v} \rangle / \partial y . \quad (1.9)$$

This is the *Taylor identity* for models 1 and 2. It is valid at any amplitude and is indifferent to whether the dynamics is ideal-fluid or not: Eq. (1.5a) was never used. It was derived by Taylor for the nondivergent barotropic case $L_D = \infty$. As just shown, however, it extends trivially to any value of L_D . It tells us that in these models the eddy flux of PV, including any contributions due to wave breaking and PV mixing, is directly tied to the eddy flux of momentum and hence to the jet dynamics. The negative-viscosity enigma has vanished in a puff of insight! It is the mixable quantity

PV that tends to go down its mean gradient — not momentum, which there is no reason to suppose is mixable.

For model 3 one replaces the momentum-flux convergence on the right of (1.9) by its counterpart in the yz plane, the convergence of an effective momentum flux whose vertical component is minus what oceanographers call the *form stress* across an undulating stratification surface due to correlations between pressure fluctuations and stratification-surface slopes. This gives the *Taylor–Bretherton identity* for model 3, first presented and used in [41]:

$$\langle \tilde{v}\tilde{q} \rangle = -\frac{\partial \langle \tilde{u}\tilde{v} \rangle}{\partial y} + \frac{1}{\rho_0} \frac{\partial}{\partial z} \left(\frac{\rho_0 f_0^2}{N^2} \left\langle \frac{\partial \phi}{\partial x} \frac{\partial \phi}{\partial z} \right\rangle \right). \quad (1.10)$$

To see that the last term contains the form stress, within the round brackets, note that $\langle \phi_x \phi_z \rangle = -\langle \phi \phi_{zx} \rangle$ and that $\rho_0 f_0 \phi$ is the pressure fluctuation while, thanks to hydrostatic balance, $-f_0 N^{-2} \phi_z$ is the stratification-surface displacement and $-f_0 N^{-2} \phi_{zx}$ its slope. For historical reasons this effective momentum flux has often been defined with a perverse sign convention and labelled the *Eliassen–Palm flux*. By the usual conventions, $-\langle \tilde{u}\tilde{v} \rangle$ ought to be minus the momentum flux or plus the stress, and similarly for the vertical, form-stress term. Like the Taylor identify (1.9), the Taylor–Bretherton identity (1.10) holds whether the dynamics is ideal-fluid or not and for disturbances of any amplitude whatever, wavelike, or turbulent, or both.

The small-amplitude pseudomomentum theorems were also derived by Taylor, Bretherton and Dickinson albeit in slightly disguised form. As things panned out historically, full clarity (in the atmosphere–ocean community) had to await introduction of what are usually called the “transformed Eulerian-mean equations” [43], shortly after which the conceptual connection with theoretical-physics principles — translational invariance, quasi-particle gases and so on — was finally made, helped by a correspondence I had with Sir Rudolf Peierls. An in-depth discussion is given in [5].

Here we define the pseudomomentum P per unit mass for small-amplitude fluctuations \tilde{q} about the translationally-invariant mean state $\langle q \rangle$, for all three models, as

$$P := -\frac{1}{2} \langle \tilde{q}^2 \rangle / \langle q \rangle_y. \quad (1.11)$$

The sign convention is chosen to make P agree with the usual ray-theoretic pseudomomentum or quasimomentum, i.e. wave action times wave vector. We expect a minus sign precisely because of the one-wayness of Rossby and drift waves.

Linearizing (1.5a) with right-hand side zero, about the mean state $\langle q \rangle$, we easily find, on multiplication by \tilde{q} and taking the zonal mean, the disturbance potential-estrophy equation $\partial_t \frac{1}{2} \langle \tilde{q}^2 \rangle = -\langle q \rangle_y \langle \tilde{v} \tilde{q} \rangle$ for all three models. The Taylor and Taylor–Bretherton identities say that we can turn the potential-estrophy equation into a conservation theorem if we divide it by $-\langle q \rangle_y$ and use the fact that, at small amplitude, we may consistently neglect the rate of mean-state evolution $\langle q \rangle_{yt}$. Thus for models 1 and 2, for instance, we have simply

$$\frac{\partial P}{\partial t} + \frac{\partial \langle \tilde{u} \tilde{v} \rangle}{\partial y} = 0 \quad (1.12)$$

which is indeed in conservation form, as is the corresponding result for model 3 for which we need only replace the second term of (1.12) by minus the right-hand side of (1.10):

$$\frac{\partial P}{\partial t} + \frac{\partial \langle \tilde{u} \tilde{v} \rangle}{\partial y} - \frac{1}{\rho_0} \frac{\partial}{\partial z} \left(\frac{\rho_0 f_0^2}{N^2} \left\langle \frac{\partial \phi}{\partial x} \frac{\partial \phi}{\partial z} \right\rangle \right) = 0. \quad (1.13)$$

Of course one can usefully repeat these derivations with the forcing or dissipation terms explicitly included on the right of (1.5a) whenever one has a particular model for those terms, such as a viscous term, or infrared radiative damping. Then one has sources and sinks of pseudomomentum P . Such sources and sinks do not necessarily require external forces to be exerted. They require only that waves be generated or dissipated somehow. This underlines the fact that pseudomomentum is not the same thing as momentum, *despite* sharing the same flux terms.

The small-amplitude pseudomomentum conservation theorems are sometimes called Charney–Drazin theorems, even though they originated in the 1915 work of Taylor [40]. The 1961 work of Charney and Drazin [44] restricted attention to steady, nondissipating waves on a special mean flow $\langle u \rangle(z)$ with vertical shear only, and vanishing horizontal shear $\langle u \rangle_y$ and Reynolds stress $\langle \tilde{u} \tilde{v} \rangle$, in model 3. Their theorem, Eqs. (8.13)ff. of [44], though influential in its time, said only that, in this special steady-waves case, the $\partial/\partial z$ term of (1.13) vanishes — the counterpart of saying that $\partial \langle \tilde{u} \tilde{v} \rangle / \partial y$ vanishes for the steady-waves case of (1.12). Unlike Taylor, they did not consider time-dependent waves and so did not find any results like (1.12) and (1.13) involving $\partial P / \partial t$.

The reader interested in deeper aspects of the theory is recommended to read the penetrating account in Bühler’s book [5]. For instance the assumption $\langle q \rangle_{yt} = 0$ used above, in order to derive (1.12) and (1.13), is consistent with the mean state being not only translationally but also temporally

invariant. Then pseudoenergy as well as pseudomomentum is conserved for ideal-fluid flow. Generically, the pseudoenergy E in a particular frame of reference can be defined as $\langle u \rangle P$ plus the positive-definite wave-energy of the linearized disturbance equations. This holds for arbitrarily-sheared mean flows $\langle u \rangle$.

Domain-integrated P and E conservation immediately give us the well known Rayleigh–Kuo–Charney–Stern and Fjørtoft shear stability theorems. The first implies stability whenever P is inherently one-signed, i.e. whenever $\langle q \rangle_y$ is one-signed, and the second whenever a translating frame of reference can be found that makes $\langle u \rangle P$ positive definite, i.e. $\langle u \rangle \langle q \rangle_y$ negative definite, even if $\langle q \rangle_y$ is two-signed. This last points to the role of counterpropagating Rossby waves in shear instabilities mentioned in Sec. 1.6. States in which $\langle q \rangle_y$ is only just one-signed (e.g. Fig. 1.1, also “PV staircases”, next section) are sometimes called “states of Rayleigh–Kuo–Charney–Stern marginal stability”, or for brevity “states of Rayleigh–Kuo marginal stability”. Beautiful generalizations and extensions of all the stability theorems were discovered by V. I. Arnol’d; see e.g. [33], [45], and references therein.

Bühler’s book [5] also makes clear to what extent one can generalize small-amplitude results like (1.12) and (1.13) to finite amplitude, for atmosphere–ocean models at least. The finite-amplitude counterparts, though conceptually important, are computationally impractical in the cases that interest us here because they require retention of Lagrangian flow information — more precisely, the shapes of originally-zonal material contours entering Kelvin’s circulation theorem. That is no great problem for waves that are not breaking, like the waves in Fig. 1.5, but becomes hopelessly complicated in turbulent zones where the waves are breaking, meaning that the material contours deforming irreversibly. It is perhaps worth noting that this difficulty has, nevertheless, been circumvented in a recent proof of a finite-amplitude version of the Rayleigh–Kuo–Charney–Stern stability theorem that is even more general than Arnold’s version, allowing fully-turbulent wave breaking and PV mixing [33], in models 1 and 3. (The Fjørtoft theorem then fails: it is easy to find counterexamples.)

It is Kelvin’s circulation theorem applied to originally-zonal material contours that accounts for the otherwise mysterious fact that, even though momentum and pseudomomentum are different physical quantities related to different translational symmetry operations, they share the same off-diagonal flux terms. Kelvin’s circulation theorem is exactly the ideal-flow constraint preventing what Diamond et al. (this volume) call “the slippage of a quasi-particle gas” of drift waves relative to the zonal flow.

We may think of the momentum-flux convergences that appear in (1.12), (1.13) and their generalizations, including the generalizations to finite disturbance amplitude, as effective wave-induced forces felt by the mean state. Such effective forces may or may not be equal to the actual mean-flow acceleration $\partial\langle u\rangle/\partial t$. If they are, then we have simply

$$\partial_t (\langle u \rangle - P) = 0 \quad (1.14)$$

for ideal-fluid flow. It can be shown that this always holds in model 2, and in model 1 for $L_D = \infty$. It is not true more generally because the response to the effective mean force normally includes implicit $O(\text{Ro})$ mean motions and mass fluxes in the y direction, whose Coriolis forces contribute to $\partial\langle u\rangle/\partial t$. In the case $L_D = \infty$, and in model 2 for all L_D , such mass fluxes are shut down by the kinematic constraints. $L_D = \infty$ models are two-dimensionally nondivergent to sufficient accuracy since with gravity $g = \infty$ we have replaced the free upper surface with a rigid lid. Otherwise it is simplest to think directly in terms of eddy fluxes of PV, focusing on the left-hand sides of the Taylor and Taylor–Bretherton identities (1.9), (1.10), and using PV inversion to calculate $\partial\langle u\rangle/\partial t$. Inversion implicitly takes full account of the implicit $O(\text{Ro})$ mean motions and mass fluxes.

For models 1–3 there are actually four momentum-like quantities that are liable to be conflated but need to be distinguished, namely (1) momentum, (2) Eulerian pseudomomentum (of which P is a simple example), (3) Lagrangian pseudomomentum (definable at finite amplitude), and (4) Kelvin impulse. Adding to the potential for confusion, the word impulse often *means* momentum in some European languages. Bühler’s book [5] keeps these distinctions clear at all stages.

It also lays out in full detail exactly how (1.14) generalizes to finite amplitude, and to atmosphere–ocean models more accurate than quasi-geostrophic, and spells out the price to be paid for such generalizations in terms of retaining the accurate Lagrangian flow information required to keep track of the shapes of material contours.

It is a nontrivial question whether or not model 2 admits any corresponding finite-amplitude results. The reason is that, in the atmosphere–ocean cases, the application of Kelvin’s circulation theorem to originally-zonal material contours requires the implicit $O(\text{Ro})$ mean motions and mass fluxes to be taken into account — that is, it requires consideration of the $O(\text{Ro})$ corrections to the leading-order velocity field $\hat{\mathbf{z}} \times \nabla\phi$. My current conjecture is that, since the zonal-mean kinematics of model 2 would appear to constrain such corrections to be zero, at least in the zonal mean, there

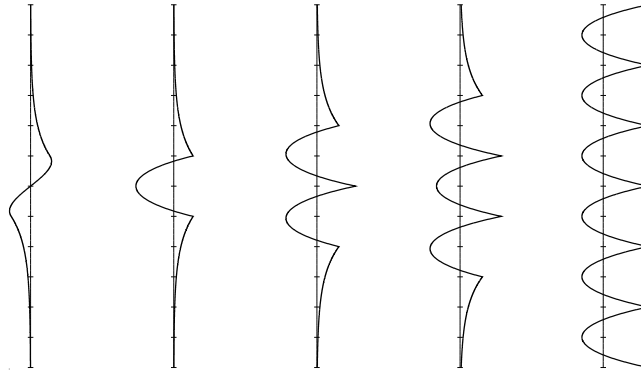


Fig. 1.7 Profiles of ϕ and u for perfect, zonally-symmetric PV staircases in model 1. Tick marks are at intervals of $y = \frac{1}{2}L = L_D$. From left to right, the first profile is that of ϕ for a single step and the second is the corresponding u profile. The remaining profiles are those of $u = -\phi_y$ for two, three and the limiting case of an infinite number of perfect steps. From [32]; q.v. for mathematical details of the inversions.

may well be a finite-amplitude counterpart to (1.14) though, if so, there is still the question of how far the Lagrangian information required might limit its usefulness in practice. However, all this would need to be checked in detail and preferably by someone who understands tokamak flows better than I do.

1.10 PV staircases

Focusing again on our main theme of strong nonlinearity, we note that the PV Phillips effect, Fig. 1.6, suggests the possible relevance of idealized saturated states consisting of perfectly mixed zones cut out of a background y -profile $q_b(y)$ having a constant gradient β (again, not to be confused with plasma beta). We take $q_b = \beta y$ as before. The graph of q against y then looks like a staircase cut out of a sloping hillside. So these idealized saturated, marginally Rayleigh–Kuo–Charney–Stern stable states are often called “PV staircases”.

The corresponding q_a profile is a zigzag. Inverting this we get an array of zonally symmetric jets whose profiles depend on the PV jump q_j at each step, as well as on the step size L , i.e. the jet spacing, in units of L_D . Some examples are shown in Fig. 1.7, for model 1 with $L/L_D = 2$ and for staircases of one, two, and three steps along with the limiting case of an infinite number of steps. The two profiles on the left are the ϕ and

u profiles for the case of one step, an idealized version of the terrestrial winter stratosphere in its usual wintertime state. The others are all u profiles. Recall that $u = -\phi_y$. The solutions are taken from [32], q.v. for mathematical details as well as for caveats regarding the conflicting uses of the term “Rhines scale”, whose relation, if any, to the jet spacing L is not as straightforward as is sometimes assumed.³

Some researchers think that the PV-staircase idealization provides a good model for Jupiter’s weather layer in extratropical latitudes — a persuasive case is made in the review article by Marcus [47] — though, hardly surprisingly, in view of our generally poor understanding of Jovian fluid dynamics, this is controversial. Alternatives have been put forward, notably by Dowling [48]. What is not in doubt is that staircase-like structures of one, two and sometimes three steps are well observed and well documented in the Earth’s atmosphere [29]. The observed states are not zonally symmetric; what they share with the simple staircase idealization are large, zonally-extensive regions of fairly well mixed PV on stratification surfaces. Those regions are bordered by narrow bands of concentrated PV gradients, the meandering jets already noted. If PV contours on a stratification surface are splayed out by mixing in some places, then they must be bunched up in others. (The only simple alternative consistent with (1.3) and its conservation properties [49] is an overwhelmingly improbable alternative, namely, to wipe out the entire pole-to-pole planetary PV gradient and thus kill the atmosphere’s rotation Ω altogether.) The simplest and clearest example of the splaying-out and bunching-up that I’m talking about is the winter stratosphere [4], [27], [28], often resembling a single-step staircase idealizable as the left-hand case in Fig. 1.7.

As L/L_D varies, the jets retain their peaked profiles, corresponding to the infinitely tight bunching of PV contours in this idealization. They change their shapes in other ways. For large L/L_D we get isolated jets, still Rayleigh–Kuo–Charney–Stern marginally stable. Figure 1.8 zooms in on one such jet, near which the q_a zigzag looks like a simple jump discontinuity, at $y = 0$, say, as shown in the right-hand graph. The zonally-symmetric inversion problem for u then simplifies to $\mathcal{L}u = u_{yy} - L_D^{-2}u = -\langle q_a \rangle_y =$

³One problem, sometimes forgotten, is that Rhines’ original concept came from a variant of homogeneous turbulence theory in which an upscale energy “cascade” is all-important, yet the Rossby waves feel only the background PV gradient β , and therefore obey the dispersion relation (1.7). Also, $L_D = \infty$ is often assumed, as in Rhines’ original work [46]. We shall see shortly that Rossby waves on PV staircases can have dispersion properties that differ substantially from (1.7), and in a way that can drastically reshape the wave–turbulence interactions.

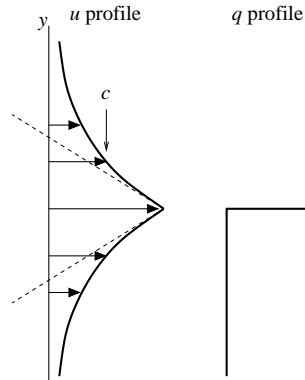


Fig. 1.8 Sketch of PV discontinuity and the corresponding velocity profile obtained by PV inversion. The step size or jet spacing L is much larger than the jet scale L_D , and we can ignore β and equate q_a and q . The solid velocity profile is from Eq. (1.15). The angle between the dashed lines is governed by the strength of the delta function $q_j \delta(y)$.

$-\langle q \rangle_y = -q_j \delta(y)$ and delivers the velocity profile shown in the left-hand graph,

$$u = \langle u \rangle = u_j \exp(-|y|/L_D) \quad (1.15)$$

where $u_j := \frac{1}{2} L_D q_j$. The dashed lines in Fig. 1.8 mark the jump in the slope u_y at the jet peak, determined by the strength of the delta function $q_j \delta(y)$ in the inversion problem. Integration of $u_{yy} - L_D^{-2} u = -q_j \delta(y)$ across $y = 0$ gives $[u_y]_{y=0^-}^{y=0^+} = -q_j$.

Staircase models are no more than an idealization, for one thing being much more deterministic than current models of the fluctuating zonal flows in tokamaks. However, it may be interesting to speculate whether, for strong nonlinearity, the staircase idealization has some relevance to the saturation problem in real tokamaks.

There is an ill-understood dependence on how the turbulence is excited. In the vast literature on numerical forced-dissipative versions of model 1 (the “beta-turbulence” literature, mostly on model 1 with $q_b = \beta y$ and $L_D = \infty$), it seems that some of the numerical experiments produce sharp staircases, e.g. [50], while others produce only a faint “washboard” (e.g. B. Galperin, personal communication). This could be partly due to the fact that differing choices of artificial forcing will disrupt PV mixing to differing extents.

Most of these studies use a prescribed stochastic external force field, rather than self-excitation. We have the same difficulty in the Jupiter

problem — a lack of clarity as to what kind of forcing or self-excitation best mimicks reality. There is also great uncertainty as to when or whether upscale energy “cascades” are involved and when, by contrast, the passive shearing of repeated PV-anomaly injections is more important [51], [52]. In “cascade” language this last produces an enstrophy but not an energy cascade. It also disrupts simple PV mixing.

The laboratory flows exemplified by Fig. 1.1 are forced in several ways that all contrive to preserve the material invariance of PV to good approximation, giving PV mixing a chance to predominate. In the experiments that produced Fig. 1.1 and similar flows, the forcings are non-stochastic, though spatially variable. In a variety of runs the outcome, in these experiments, always seems to be robustly a flow like that in Fig. 1.1, a prograde jet that is “staircase-like” in the same sense as the flow in Fig. 1.8.

In these experiments, forcing and dissipation are kept far weaker than in most laboratory experiments. The tank in Fig. 1.1 is unusually large — 86.4cm in diameter — and can be rotated unusually fast without disintegrating, up to 4 revolutions per second. Figure 1.1 used 3 per second, $|\mathbf{\Omega}| = 18.8\text{s}^{-1}$. So the wave–turbulence interactions that shape the flow are almost free of forcing and dissipation. See [11] and [12] for more details.

The only other laboratory experiments with comparable weakness of forcing and dissipation, of which I’m aware, are those of Read et al. [53]. They use an ingenious quasi-stochastic forcing method in an extremely large tank, 13m diameter, though at much smaller $|\mathbf{\Omega}|$. Meandering jets are obtained, and temporary local reversals of PV gradients “indicative of Rossby wave breaking”, though in the absence of PV maps like those in [11] and [12] it is hard to make a closer assessment. It appears, however, that in these experiments the turbulence is too weak to bring the system close to a well developed staircase-like regime. In this connection some current numerical experiments by R. K. Scott and D. G. Dritschel are noteworthy, in that they are beginning to clarify the precise forcing and dissipation parameter ranges conducive to staircasing [54].

T. E. Dowling and co-workers have argued that Jupiter may be different again, possibly close to a state that is marginal not by the Rayleigh–Kuo–Charney–Stern stability criterion but, rather, by that of Arnol’d’s Second Theorem. The q profiles would then be “hyperstaircase-like” to the extent that they have reversed PV gradients. There is some indirect, but I think persuasive, observational evidence that Jupiter’s weather layer may be close to such a state [48]. But the question of what forcing mechanisms might lead to it does not yet seem to have been clearly answered — though

an extremely promising candidate, direct forcing by moist (thunderstorm) convection, has been put forward from time to time and is now under intensive investigation, e.g. [55], [56], and references therein. This suggests a leading role for the passive shearing of repeated PV-anomaly injections [51], [52], the simplest mechanism able to overcome PV-mixing tendencies and produce a hyperstaircase.

1.11 Jet self-sharpening and meandering: a toy model

The single isolated jet in Fig. 1.8 is the simplest of all Rossby waveguides. Its dispersion relation differs substantially from (1.7), and in a way that will prove interesting. It signals a kind of wave-turbulence, linear-nonlinear interaction that differs greatly from the standard homogeneous-turbulent Rhines

Linearizing (1.5a) with right-hand side zero about the profiles in Fig. 1.8, with \mathcal{L} defined as in (1.6a), and continuing to drop the suffix g , we have

$$\tilde{q}_t + \langle u \rangle \tilde{q}_x + \langle q \rangle_y \tilde{\phi}_x = 0 \quad (1.16)$$

where $\langle u \rangle$ is given by (1.15), and $\langle q \rangle_y = q_j \delta(y)$ as before. For a disturbance of the standard form $\tilde{\phi} \propto \hat{\phi}(y) \exp\{ik(x - ct)\}$, with phase velocity c and wavenumber k along the jet, we have from (1.6a)

$$\tilde{q} = \mathcal{L}\tilde{\phi} = \tilde{\phi}_{yy} - (k^2 + L_D^{-2})\tilde{\phi}. \quad (1.17)$$

So, with $\hat{q} := \hat{\phi}_{yy} - (k^2 + L_D^{-2})\hat{\phi}$, (1.16) implies when $k \neq 0$ that

$$(\langle u \rangle - c) \hat{q} + q_j \delta(y) \hat{\phi} = 0, \quad (1.18)$$

integration of which across $y = 0$ gives

$$(u_j - c) \left[\hat{\phi}_y \right]_{y=0-}^{y=0+} + q_j \hat{\phi}|_{y=0} = 0 \quad (1.19)$$

for the jump in $\hat{\phi}_y$ across $y = 0$. Away from $y = 0$, we have $\langle q \rangle_y = 0$ hence $\hat{q} = 0$ and therefore

$$\hat{\phi}(y) \propto \exp\{-(k^2 + L_D^{-2})^{1/2}|y|\}. \quad (1.20)$$

For (1.19) and (1.20) to be compatible we must have, with $u_j = \frac{1}{2}L_D q_j$,

$$c = u_j \{1 - (1 + L_D^2 k^2)^{-1/2}\}, \quad (1.21)$$

which may be compared with (1.7), which has no square root in its denominator $L_D^{-2} + k^2 + l^2$. The square root in (1.21) arises from the infinite

bunching of PV contours at the jet core, giving dispersion properties distinctly different from those where the background PV contours are evenly spread out, as assumed in (1.7) and in its limiting case $L_D^2 \rightarrow \infty$ used in the standard Rhines-scale argument.

In (1.21) notice especially that, as k varies monotonically between 0 and ∞ , c varies monotonically between 0 and u_j . That is, for this jet there are always “critical lines” — that is, y values such that $\langle u \rangle = c$ — on each flank of the jet as indicated in Fig. 1.8. Thus, whenever the jet is disturbed, the undulations of its core will inevitably give rise to PV mixing on either side. In a frame of reference moving with the wave at speed c , one sees Kelvin-cat’s-eye flow patterns in the jet flanks, which must twist up any stray PV contours like spaghetti on a fork. Whenever the undulations increase in amplitude, the widths of the mixing regions expand, tending on average to keep the PV contours bunched up in the core and maintaining the eddy-transport barrier there, in the typical way.

The presence of more than one zonal wavenumber k complicates the kinematical details, going over to Kelvin sheared-disturbance kinematics [51] for broad spectra. But none of this can suppress the PV mixing in the jet flanks. This is the typical antifrictional jet self-sharpening process and, broadly speaking, is the kind of kinematics already encountered in Fig. 1.1 and in the other examples mentioned. It is typical of the real, highly inhomogeneous wave–turbulence interactions observed in the atmosphere and oceans — see also [57] for a good discussion of some oceanic examples — with linear, wavelike regions closely adjacent to fully nonlinear, wave-breaking regions. It is well verified in fully nonlinear numerical experiments, e.g. [58], [59]. As already emphasized, it is at an opposite extreme from a homogeneous-turbulence scenario using (1.7) as the Rossby-wave dispersion relation. Further discussion and further illustrations can be found for instance in [17], [30], and [33].

The long-wave behaviour is relevant to the issue of meandering. If we take $k^2 \ll L_D^{-2}$ in (1.21) we find phase and group velocities

$$c \approx \frac{1}{2}u_j L_D^2 k^2, \quad c_{\text{group}} \approx \frac{3}{2}u_j L_D^2 k^2 \quad (1.22)$$

that match the jet’s surrounding flow velocity $\langle u \rangle \approx 0$ for sufficiently small k^2 . This says that a meandering jet flows through its surroundings almost like a river. Large-scale meanders have very little propensity to propagate upstream or downstream. The same thing holds even for large-amplitude meanders, and for generalizations of model 1 beyond quasi-geostrophic theory, as shown in [60]. The meandering behaviour of a nonlinear version

of our isolated-jet model is strikingly reminiscent of the large-scale, large-amplitude meandering of real atmosphere-ocean jets. The nonlinear model even succeeds in mimicking the cutoff behaviour that sheds Gulf-stream rings. Again, further discussion is in [17].

It is worth remarking that the long-wave dispersion properties just described do not depend on having an idealized, perfectly sharp jet, with infinitely close bunching of its PV contours — at least not within linear theory. As long as $\langle q \rangle_y = \langle u \rangle_{yy} - L_D^{-2} \langle u \rangle$ to sufficient accuracy — which means continuing to neglect the planetary-scale background contribution β — and as long as the jet velocity profile $\langle u \rangle$ approaches zero on either side of the jet core, we always find phase speeds c that also approach zero as $k^2 \rightarrow 0$. This can be seen by inspection of (1.16)–(1.17). As long as k^2 can be neglected in (1.17), the disturbance problem (1.16) evidently has a solution $\hat{\phi} \propto \langle u \rangle$ with $c = 0$. This fact was pointed out in [61] and extensively exploited for planetary-scale Rossby waves on a strongly-sheared stratospheric polar-night jet in [62]. The physical reason is that the long-wavelength meanders tend to take place with all the jet's PV contours moving as one, as long as they are sufficiently bunched to avoid further mixing by the wave breaking on either side.

How much of this carries over to model 2? The general long-wave solution just described fails; but in the idealized sharp-jet case we get precisely the same dispersion properties, (1.21)–(1.22), as in model 1, despite having a very different jet velocity profile. In model 2 the sharp-jet velocity profile is given by the pair of dashed lines on the left of Fig. 1.8. (Model 2, with the same PV jump q_j , requires us to set $L_D = \infty$ in the local inversion problem for the jet profile, i.e. to set $L_D = \infty$ in $\langle u \rangle_{yy} - L_D^{-2} \langle u \rangle = \langle u \rangle_{yy} = -q_j \delta(y)$, which is satisfied by the pair of dashed lines.)

The derivation (1.16)–(1.22) of the linear wave theory applies word for word and symbol for symbol, provided that u_j still denotes the maximum jet velocity. With $\hat{q} = 0$ everywhere except for the delta function at $y = 0$, advection $\langle u \rangle \partial_x$ by the the mean flow $\langle u \rangle$ has no role away from $y = 0$.

The dashed lines in Fig. 1.8 are of course only a local approximation within a full staircase with large step size L ; it is easy to show by restoring the β contribution to q_y that the dashed lines are really part of a set of larger-scale parabolic profiles, qualitatively like the profiles in Fig. 1.7 though shifted to the left. Again, details are given in [32]. All that matters for the present discussion is that the range of $\langle u \rangle$ values expands when we go from model 1 to model 2, and in particular that model 2 still has the property noted above that critical lines $\langle u \rangle = c$ will always be present.

1.12 Concluding remarks

The river-like, meandering behaviour of isolated jets in model 1 and the small long-wave phase and group velocities in (1.22) point to a certain dynamical flaccidity of these jets. Their quasi-elasticity is not very effective at long wavelengths. This is related to the short range of the interaction described by the inversion kernel K_0 in (1.8). The short interaction range also affects vortex interactions and any resulting PV mixing, as illustrated for instance by ultra-high-resolution turbulence simulations in [30].

Model 2 has the same inversion kernel K_0 for all non-zonal motions $\tilde{\phi}$. So it should exhibit similar flaccidity and jet meandering. Model 2 also has a similar antifrictional jet self-sharpening mechanism, albeit confined more closely to the neighbourhood of the jet core thanks to its jet velocity profiles being more like the dashed than the solid curves on the left of Fig. 1.8. The different jet velocity profiles imply, however, that “river-like” is no longer a good description. I am not sure how important this distinction might be.

I wonder, though, to what extent we can take model 2 itself at face value. As argued in Sec. 1.8, the standard two-layer counterpart of model 1 might be a closer cousin to the real tokamak. That in turn would make Jupiter a far more distant cousin, contrary to what is sometimes suggested, if only because of the very different excitation — almost certainly *not* baroclinic instability or other self-excitation but, much more likely, I now think, external forcing by sheared thunderstorm injections at much smaller scales.

Acknowledgements

I am very grateful to Laurène Jouve and Chris McDevitt for producing the first draft and to Steve Cowley, Pat Diamond and Philippe Ghendrih for patiently explaining some aspects of tokamak dynamics, and for help with the plasma literature and its notational conventions. Tim Dowling, Peter Read and Richard Wood have helped me with recent developments in Jovian dynamics, real and idealized. Huw Davies helped with recent terrestrial developments and Steven Balbus and Toby Wood with solar.

Bibliography

- [1] P. H. Diamond, S.-I. Itoh, K. Itoh, and T. S. Hahm. Zonal flows in plasmas — a review. *Plasma Phys. Control. Fusion*, 47:R35–R161, 2005.
- [2] P. W. Terry. Suppression of turbulence and transport by sheared flow. *Rev. Mod. Phys.*, 72:109–165, 2000.
- [3] M. E. McIntyre and T. N. Palmer. Breaking planetary waves in the stratosphere. *Nature*, 305:593–600, 1983.
- [4] M. E. McIntyre. Tachocline fluid dynamics: an interim assessment. conference talk with movies, in: *Wave and Physics*, a conference in honour of Professor Douglas Gough, on the occasion of his 70th birthday, Centro de Astrofísica da Universidade do Porto, <https://www.astro.up.pt/investigacao/conferencias/dog2011/index.php?opt=programme>. Also “survey talk” at <http://www.atm.damtp.cam.ac.uk/people/mem/tachocline/>, 2011.
- [5] O. Bühler. *Waves and Mean Flows*. University Press, Cambridge, 2009.
- [6] E. N. Lorenz. *The Nature and Theory of the General Circulation of the Atmosphere*. World Meteor. Org., Geneva, 1967.
- [7] V. P. Starr. *Physics of negative viscosity phenomena*. McGraw-Hill, 1968.
- [8] J. H. Rogers. *The Giant Planet Jupiter*. Cambridge University Press, 1995.
- [9] M. N. Jukes and M. E. McIntyre. A high resolution, one-layer model of breaking planetary waves in the stratosphere. *Nature*, 328:590–596, 1987.
- [10] E. F. Danielsen. Stratospheric-tropospheric exchange based on radioactivity, ozone and potential vorticity. *J. Atmos. Sci.*, 25:502–518, 1968.
- [11] J. Sommeria, S. D. Meyers, and H. L. Swinney. Laboratory model of a planetary eastward jet. *Nature*, 337:58–61, 1989.
- [12] J. Sommeria, S. D. Meyers, and H. L. Swinney. Experiments on vortices and Rossby waves in eastward and westward jets. In A. R. Osborne, editor, *Nonlinear Topics in Ocean Physics*, pages 227–269, Amsterdam, 1991. North-Holland.
- [13] W. A. Norton. Breaking Rossby waves in a model stratosphere diagnosed by a vortex-following coordinate system and a technique for advecting material contours. *J. Atmos. Sci.*, 51:654–673, 1994.
- [14] D. W. Waugh and R. A. Plumb. Contour advection with surgery: a technique for investigating finescale structure in tracer transport. *J. Atmos. Sci.*,

- 51:530–540, 1994.
- [15] H. Riehl. *Jet Streams of the Atmosphere*. Colorado State University, Fort Collins, CO., USA, 1962. Tech Paper No. 32.
- [16] E. Palmén and C. Newton. *Atmospheric Circulation Systems*. Academic Press, 1969.
- [17] M. E. McIntyre. Potential-vorticity inversion and the wave-turbulence jigsaw: some recent clarifications. *ADGEO (Advances in Geosciences)*, 15:47–56, 2008.
- [18] C.-G. Rossby. Dynamics of steady ocean currents in the light of experimental fluid mechanics. *Mass. Inst. of Technology and Woods Hole Oceanogr. Instn., Papers in Physical Oceanography and Meteorology*, 5(1):1–43, 1936.
- [19] C.-G. Rossby. Planetary flow patterns in the atmosphere. *Q. J. Roy. Meteorol. Soc.*, 66 (Suppl.):68–87, 1940.
- [20] H. Ertel. Ein neuer hydrodynamischer Wirbelsatz. *Met. Z.*, 59:271–281, 1942.
- [21] J. G. Charney. On the scale of atmospheric motions. *Geofysiske Publ.*, 17(2):3–17, 1948.
- [22] A. M. Obukhov. On the problem of the geostrophic wind. *Izv. Akad. Nauk SSSR, Ser. Geograf. Geofiz.*, 13(4):281–306, 1949. in Russian.
- [23] E. Kleinschmidt. Über Aufbau und Entstehung von Zyklonen (1 Teil). *Meteorol. Rund.*, 3:1–6, 1950.
- [24] B. J. Hoskins, M. E. McIntyre, and A. W. Robertson. On the use and significance of isentropic potential-vorticity maps. *Q. J. Roy. Meteorol. Soc.*, 111:877–946, 1985.
- [25] C. D. Thorncroft, B. J. Hoskins, and M. E. McIntyre. Two paradigms of baroclinic-wave life-cycle behaviour. *Q. J. Roy. Meteorol. Soc.*, 119:17–55, 1993.
- [26] C. Appenzeller, H. C. Davies, and W. A. Norton. Fragmentation of stratospheric intrusions. *J. Geophys. Res.*, 101:1435–1456, 1996.
- [27] M. E. McIntyre. How well do we understand the dynamics of stratospheric warmings? *J. Meteorol. Soc. Japan*, 60:37–65, 1982. Special Centennial Issue *Frontiers of Atmospheric Sciences*, ed. K. Ninomiya. Note that “latitude” was misprinted as “altitude” on page 39a line 2.
- [28] M. Riese, G. L. Manney, J. Oberheide, X. Tie, R. Spang, and V. Küll. Stratospheric transport by planetary wave mixing as observed during CRISTA-2. *J. Geophys. Res.*, pages 107(D23), pp, 2002.
- [29] O. Martius, C. Schwierz, and H. C. Davies. Tropopause-level waveguides. *J. Atmos. Sci.*, 67:866–879, 2010.
- [30] D. G. Dritschel and R. K. Scott. Jet sharpening by turbulent mixing. *Phil. Trans. R. Soc. A*, 369:754–770, 2011.
- [31] M. E. McIntyre and T. N. Palmer. A note on the general concept of wave breaking for Rossby and gravity waves. *Pure Appl. Geophys.*, 123:964–975, 1985.
- [32] D. G. Dritschel and M. E. McIntyre. Multiple jets as PV staircases: the Phillips effect and the resilience of eddy-transport barriers. *J. Atmos. Sci.*, pages 855–874., 2008.

- [33] R. B. Wood and M. E. McIntyre. A general theorem on angular-momentum changes due to potential vorticity mixing and on potential-energy changes due to buoyancy mixing. *J. Atmos. Sci.*, 67:1261–1274, 2010.
- [34] O. M. Phillips. Turbulence in a strongly stratified fluid — is it unstable? *Deep Sea Res.*, 19:79–81, 1972.
- [35] P. H. Haynes, D. A. Poet, and E. F. Shuckburgh. Transport and mixing in kinematic and dynamically-consistent flows. *J. Atmos. Sci.*, 64:3640–3651, 2007.
- [36] B. R. Ruddick, T. J. McDougall, and J. S. Turner. The formation of layers in a uniformly stirred density gradient. *Deep Sea Res.*, 36:597–609, 1989.
- [37] M. Wakatani and A. Hasegawa. A collisional drift wave description of plasma edge turbulence. *Phys. Fluids*, 27:611–618, 1984.
- [38] F. P. Bretherton. Baroclinic instability and the short wavelength cut-off in terms of potential vorticity. *Q. J. Roy. Meteorol. Soc.*, 92:335–345, 1966.
- [39] A. F. Thompson and W. R. Young. Two-layer baroclinic eddy heat fluxes: zonal flows and energy balance. *J. Atmos. Sci.*, 64:3214–3231, 2007.
- [40] G. I. Taylor. Eddy motion in the atmosphere. *Phil. Trans. Roy. Soc. Lond.*, A215:1–23, 1915.
- [41] F. P. Bretherton. Critical layer instability in baroclinic flows. *Q. J. Roy. Meteorol. Soc.*, 92:325–334, 1966.
- [42] R. E. Dickinson. Theory of planetary wave-zonal flow interaction. *J. Atmos. Sci.*, 26:73–81, 1969.
- [43] D. G. Andrews and M. E. McIntyre. Planetary waves in horizontal and vertical shear: the generalized Eliassen–Palm relation and the mean zonal acceleration. *J. Atmos. Sci.*, 33:2031–2048, 1976.
- [44] J. G. Charney and P. G. Drazin. Propagation of planetary-scale disturbances from the lower into the upper atmosphere. *J. Geophys. Res.*, 66:83–109, 1961.
- [45] M. E. McIntyre and T. G. Shepherd. An exact local conservation theorem for finite-amplitude disturbances to nonparallel shear flows, with remarks on Hamiltonian structure and on Arnol’d’s stability theorems. *J. Fluid Mech.*, 181:527–565, 1987.
- [46] P. B. Rhines. Waves and turbulence on a beta-plane. *J. Fluid Mech.*, 69:417–443, 1975.
- [47] P. S. Marcus. Jupiter’s Great Red Spot and other vortices. *Ann. Rev. Astron. Astrophys.*, 31:523–573, 1993.
- [48] T. E. Dowling. A relationship between potential vorticity and zonal wind on jupiter. *J. Atmos. Sci.*, 50:14–22, 1993.
- [49] P. H. Haynes and M. E. McIntyre. On the conservation and impermeability theorems for potential vorticity. *J. Atmos. Sci.*, 47:2021–2031, 1990.
- [50] S. Danilov and D. Gurarie. Scaling, spectra and zonal jets in β -plane turbulence. *Phys. Fluids*, 16:2592–2603, 2004.
- [51] W. Thomson (Lord Kelvin). Stability of fluid motion — rectilinear motion of viscous fluid between two parallel planes. *Phil. Mag.*, 24:188–196, 1887.
- [52] B. F. Farrell and P. J. Ioannou. Structure and spacing of jets in barotropic turbulence. *J. Atmos. Sci.*, 64:3652–3665, 2007.
- [53] P. L. Read, Y. H. Yamazaki, S. R. Lewis, P. D. Williams, R. Wordsworth,

- K. Miki-Yamazaki, J. Sommeria, and H. Didelle. Dynamics of convectively driven banded jets in the laboratory. *J. Atmos. Sci.*, 64:4031–4052, 2007.
- [54] R. K. Scott and D. G. Dritschel. The structure of zonal jets in geostrophic turbulence. *J. Fluid Mech*, 2011. Submitted; preprint at www.vortex.mcs.st-and.ac.uk/~rks/publications.html.
- [55] A. P. Ingersoll, P. J. Gierasch, D. Banfield, W. R. Vasavada, and the Galileo Imaging Team. Moist convection as an energy source for the large-scale motions in Jupiter’s atmosphere. *Nature*, 403:630–632, 2000.
- [56] Y. Lian and A.P. Showman. Generation of equatorial jets by large-scale latent heating on the giant planets. *Icarus*, 207:373–393, 2010.
- [57] C. W. Hughes. The Antarctic Circumpolar Current as a waveguide for Rossby waves. *J. Phys. Oceanogr.*, 26:1375–1387, 1996.
- [58] M. D. Greenslade and P. H. Haynes. Vertical transition in transport and mixing in baroclinic flows. *J. Atmos. Sci.*, 65:1137–1157, 2008.
- [59] J. G. Esler. The turbulent equilibration of an unstable baroclinic jet. *J. Fluid Mech.*, 599:241–268, 2008.
- [60] J. Nycander, D. G. Dritschel, and G. G. Sutyrin. The dynamics of long frontal waves in the shallow water equations. *Phys. Fluids*, 5(5):1089–1091, 1993.
- [61] P. G. Drazin and L. N. Howard. The instability to long waves of unbounded parallel inviscid flow. *J. Fluid Mech.*, 14:257–283, 1962.
- [62] A. J. Simmons. Planetary-scale disturbances in the polar winter stratosphere. *Q. J. Roy. Meteorol. Soc.*, 100:76–108, 1974.